JACS
JOURNAL OF THE AMERICAN CHEMICAL SOCIETY
Article
pubs.acs.org/JACS

Extremely Strong Self-Assembly of a Bimetallic Salen Complex Visualized at the Single-Molecule Level

Giovanni Salassa,[†] Michiel J. J. Coenen,[‡] Sander J. Wezenberg,[†,⊥] Bas L. M. Hendriksen,[‡] Sylvia Speller,[‡] Johannes A. A. W. Elemans,*[,‡] and Arjan W. Kleij*[,†,§]

[†]Institute of Chemical Research of Catalonia (ICIQ), Av. Països Catalans 16, 43007, Tarragona, Spain
[‡]Radboud University Nijmegen, Institute for Molecules and Materials, Heyendaalseweg 135, 6525 AJ Nijmegen, The Netherlands
[§]Catalan Institute for Research and Advanced Studies (ICREA), Pg. Lluis Companys 23, 08010, Barcelona, Spain

Supporting Information

ABSTRACT: A bis-Zn(salphen) structure shows extremely strong self-assembly both in solution as well as at the solid–liquid interface as evidenced by scanning tunneling microscopy, competitive UV–vis and fluorescence titrations, dynamic light scattering, and transmission electron microscopy. Density functional theory analysis on the Zn_2 complex rationalizes the very high stability of the self-assembled structures provoked by unusual oligomeric $(Zn–O)_n$ coordination motifs within the assembly. This coordination mode is strikingly different when compared with mononuclear Zn(salphen) analogues that form dimeric structures having a typical Zn_2O_2 central unit. The high stability of the multinuclear structure therefore holds great promise for the development of stable self-assembled monolayers with potential for new opto-electronic materials.

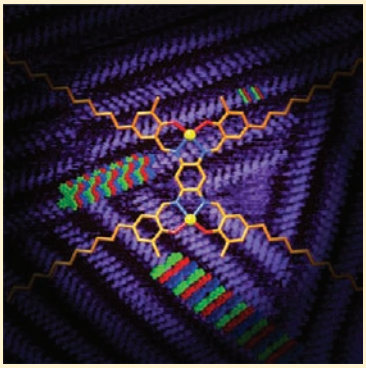

INTRODUCTION

Supramolecular aggregation or polymerization[1] is a vibrant area of research providing materials that are interesting for nanofabrication,[2] self-healing,[3] and electronic[4] applications. The use of noncovalent interactions in these polymers allows generally for a reversible assembly process, which is influenced by external stimuli, such as temperature, solvent polarity, and additives. Whereas hydrogen bonding has been extensively used for supramolecular oligo- and polymerization of organic monomers,[5] metal coordination driven self-assembly has also demonstrated to be extremely useful in this area, especially for π-conjugated molecules, such as porphyrin-based architectures.[6] The formation of highly stable self-assembled monolayers (SAMs) based on π-conjugated systems is particularly attractive in the development of functional patterned surfaces for electronic applications.[2] Crucial in these type of materials is the alignment of the molecular components and the overall stability of the system, a combination that is very difficult to control.

Previously, we have described the self-assembly of mononuclear metallosalphen complexes (**8** and **9**; see Scheme 1) at the solid–liquid interface.[7] Whereas coordinatively saturated Ni-centered complexes exclusively organize into monolayers, their Zn analogues give unusual bilayers. This is the result of strong dimerization through μ_2-phenoxo (Zn–O) bridging.[8] Furthermore, it has been demonstrated that the addition of small amounts of competitively binding pyridine (Py) easily disrupts the Zn(salphen) dimer. Recently, we have also reported that a higher nuclearity (i.e., more Zn(salphen) units per molecule) results in an up to six-fold increase in the overall stability of the formed assemblies.[9]

Scheme 1. Bimetallic Salphens 1–7 and Mononuclear Analogues 8–10

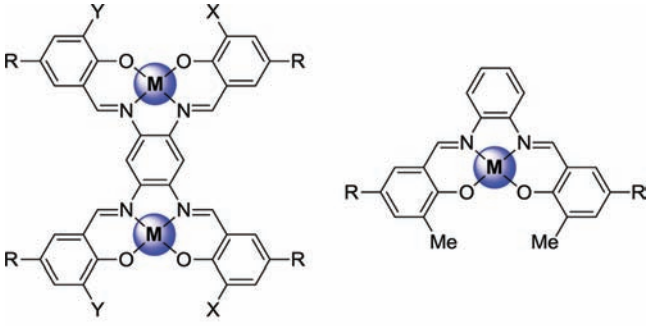

1. R = $C_{12}H_{25}$; Y = X = Me; M = Zn
2. R = $C_{12}H_{25}$; Y = X = Me; M = Ni
3. R = H; Y = X = Me; M = Zn
4. R = H; Y = X = allyl; M = Zn
5. R = H; Y = NO_2, X = CF_3; M = Zn
6. R = H; Y = NO_2, X = allyl; M = Zn
7. R = H; Y = X = tBu; M = Zn

8. R = $C_{12}H_{25}$; M = Zn
9. R = $C_{12}H_{25}$; M = Ni
10. R = H; M = Zn

Herein, we report on the unique self-assembly behavior of bis-Zn(salphen) [salphen = *N*,*N*′-bis-salicylidene-1,2-diaminobenzene] molecules **1** and **3**–**6** (Scheme 1) into extremely

Received: March 30, 2012
Published: April 4, 2012

   dx.doi.org/10.1021/ja3030802 | *J. Am. Chem. Soc.* 2012, 134, 7186–7192

stable oligomeric stacks both in the solution phase as well as at the solid–liquid interface. The aggregation of these dinuclear compounds was investigated by scanning tunneling microscopy (STM), competitive UV–vis and fluorescence titrations, dynamic light scattering (DLS), and transmission electron microscopy (TEM). Molecular modeling and density functional theory (DFT) analysis have additionally been used to elucidate the involved coordination mode, which point at the presence of single Zn–O interactions, where each metal center in the aggregated species is axially coordinated by an oxygen donor from another bis-salphen complex.

RESULTS AND DISCUSSION

Synthesis of bis-M(salphen) Complexes. The bis-Zn(salphen) complexes **1** and **3** were prepared using similar methods as previously communicated for dinuclear **4**–**7**[10] and mononuclear **8**–**10** (Scheme 1).[7,8] The bis-Ni analogue **2** was obtained after trans-metalation of **1** using $Ni(OAc)_2{\cdot}4H_2O$ (see Supporting Information for details).

STM Studies. The aggregation behavior of dinuclear **1** (Zn_2) and **2** (Ni_2) was first studied at the molecular level using STM (Figures 1 and 2 and Supporting Information).

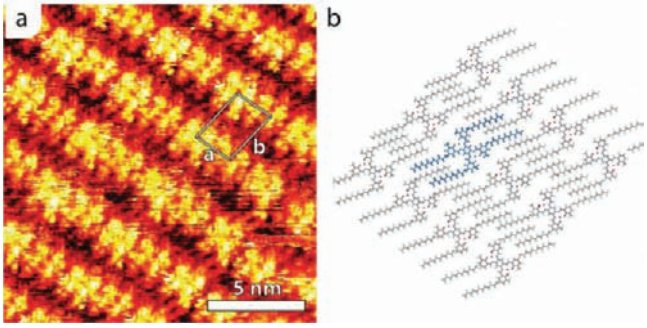

Figure 1. (a) STM topography image of a monolayer of bis-Ni(salphen) complex **2** at the HOPG–TCB interface, V_{bias} = −550 mV, i_{set} = 16 pA, and concentration [**2**] ≈ 10^{-4} M; the unit cell is indicated in white. (b) Proposed organization of the molecules of **2** in the monolayer, in which one of the molecules is colored blue for clarity. The conjugated parts of the molecule, which appear bright in the STM image, are submolecularly resolved, and the square shapes of these bright parts clearly show the internal structure of the bis-salphen moieties in **2**.

Experiments were carried out in which the bis-salphen complexes **1** and **2** were self-assembled at the interface of highly oriented pyrolytic graphite (HOPG) and 1,2,4-trichlorobenzene (TCB). In separate experiments, a droplet of a solution of each of the compounds was brought onto a piece of freshly cleaved graphite, and subsequently topography images were recorded by immersing the STM tip in this droplet. STM images of the monolayer of the bis-Ni(salphen) **2** reveal that the molecules are adsorbed with their extended conjugated surfaces parallel to the graphite surface (Figure 1a). The unit cell was determined to be a = (2.1 ± 0.2) nm, b = (3.0 ± 0.2) nm, and α = (80 ± 4)°. While the conjugated parts of the molecule, which appear bright in the STM image, are submolecularly resolved, the alkyl chains are only partly resolved and situated in the dark regions between the cores of **2**. The square shapes of the bright parts clearly show the internal structure of the bis-salphen moieties. A molecular model of the proposed organization of **2** at the surface, based on the unit cell parameters, is shown in Figure 1b.

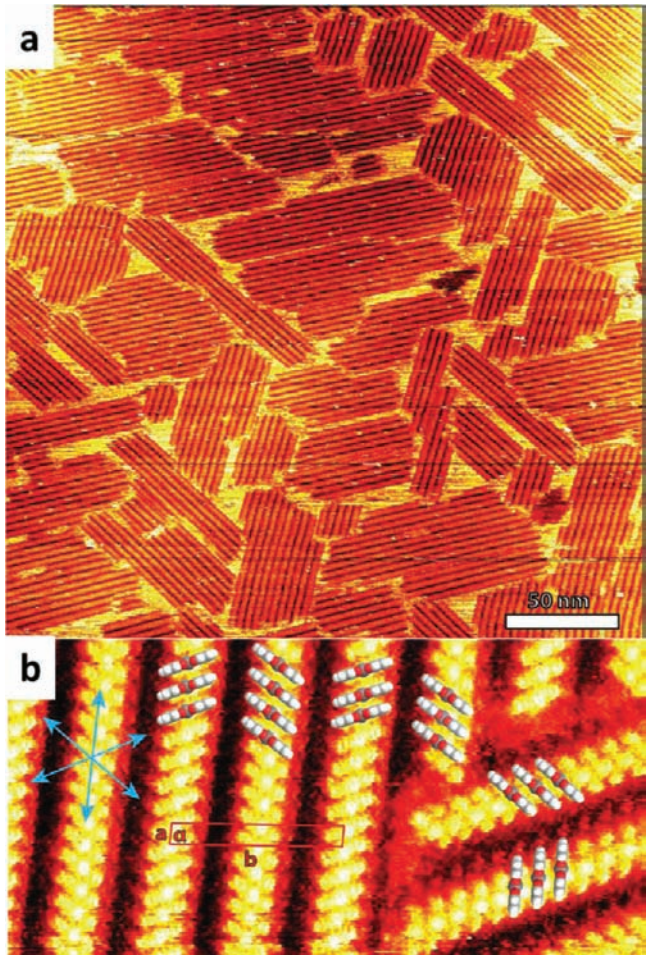

Figure 2. (a) STM topography image overviewing a monolayer of bis-Zn(salphen) complex **1** at the HOPG–TCB interface. V_{bias} = −366 mV, i_{set} = 7 pA; [**1**] ≈ 10^{-4} M. (b) STM topography image of a monolayer of **1** at the interface of HOPG and TCB/THF 95:5 (v/v); V_{bias} = −750 mV, i_{set} = 19 pA; some molecular models of **1** are superimposed (alkyl chains have been omitted and the orientation of the aromatic cores is tentatively proposed); in red the unit cell is depicted, and the blue arrows indicate the <1 −1 0 0 > symmetry vectors of the underlying graphite surface.

In strong contrast to the molecules of **2**, those of bis-Zn(salphen) **1** were found to self-assemble exclusively with their extended conjugated surfaces perpendicular to the HOPG–TCB interface. In the STM images (Figure 2 and Figures S2–5, Supporting Information), extended domains of long lamellar arrays (stacks) of molecules of **1** are visible, which are directed along one of the HOPG symmetry directions. In these arrays, the bright salphen cores are rotated under an angle of ±60° with respect to the lamellar direction, and this rotation is reversed in every other lamella. Both the direction of the arrays and the specific rotation of the salphen planes indicate a significant interaction of the molecules with the underlying graphite lattice. The alkyl tails reside in the dark areas in the STM images and are not well-resolved. Only very occasionally a defect in the form of missing molecules was observed (an example of such a defect is visible in Figure S2, Supporting Information). The unit cell contains two molecules of **1** (Figure 2b). Its parameters have been determined by coimaging the monolayer together with the underlying graphite lattice and are

dx.doi.org/10.1021/ja3030802 | J. Am. Chem. Soc. 2012, 134, 7186–7192

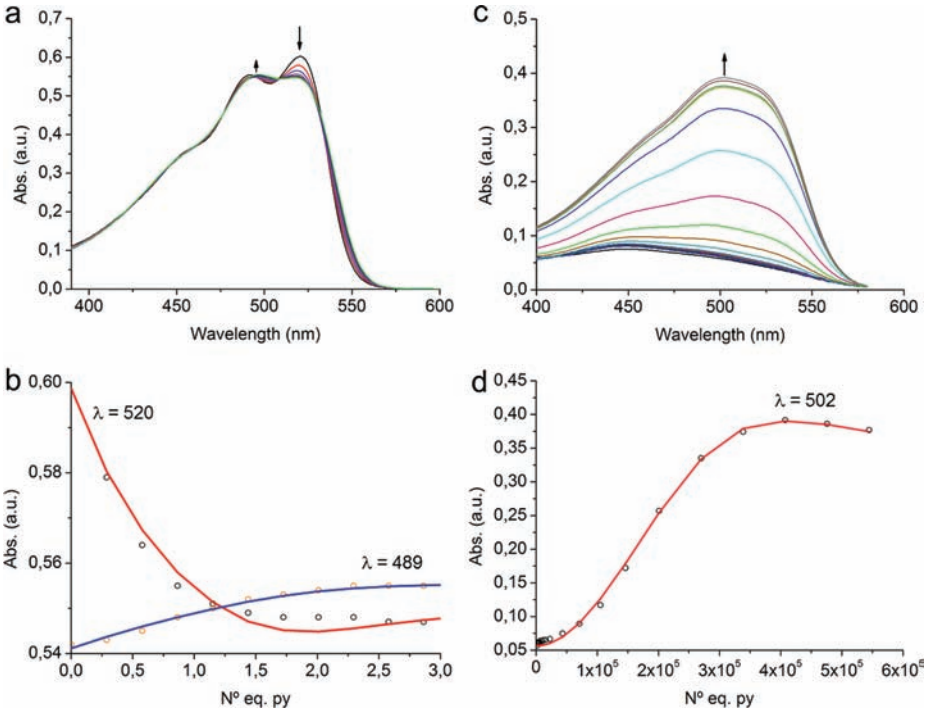

Figure 3. At the left: (a) Spectral changes of complex **7** upon the addition of pyridine carried out in toluene at $[7] = 0.95 \times 10^{-5}$ M. (b) The corresponding titration curves and data fits at $\lambda = 498$ and 520 nm. At the right: (c) Spectral changes of complex **1** upon the addition of pyridine carried out in toluene at $[\mathbf{1}] = 0.9 \times 10^{-5}$ M. (d) The corresponding titration curves and data fit at $\lambda = 502$ nm for $n = 4$. See for further details the Supporting Information.

$a = (0.87 \pm 0.04)$ nm, $b = (6.4 \pm 0.1)$ nm, and $\alpha = (87.9 \pm 0.9)°$.

The difference in coordination behavior between the penta-coordinate Zn centers in **1** and the coordinatively saturated, tetra-coordinate Ni centers in **2** is clearly reflected in the self-assembly at the surface. The observed stacking behavior of the edge-on-oriented molecules of bis-Zn(salphen) **1** is not only in complete contrast with the 2D self-assembly of the bis-Ni(salphen) **2** but also with that of previously investigated mononuclear Zn(salphen) complexes, which were found to adsorb exclusively with their aromatic planes face-on at the solid–liquid interface.[7] Previous STM studies revealed that stacks of cyclic zinc porphyrin oligomers are also arranged edge-on at the solid–liquid interface in a similar close-packed arrangement as **1**.[11] These stacks could be readily dissociated by adding ≈10 equivalents of pyridine or 4,4′-bipyridine derivatives, which acted as disruptive axial ligands for the zinc centers.

To investigate the stability of the stacked structures of **1**, STM experiments were carried out in which droplets of solutions containing potential axial ligands for the Zn centers were added in situ to the solid–liquid interface. Neither the addition of TCB solutions containing a 100-fold excess of 4,4′-bipyridine or 4-pyridylmethyloxo-diphenyl-*tert*-butylsilane (Figure S3, Supporting Information) nor the addition of 5% (v/v) of THF (an oxygen-donating axial ligand for **1**) to the TCB solvent (Figure 2b) resulted in any visible dissociation of the stacks with STM or a detectable change in the unit cell parameters. This might be caused by the rigidity of the stacks adsorbed to the surface, which would inhibit penetration of the axial ligands between the individual molecules of **1** due to steric reasons. However, when the solutions of **1** and axial ligand were premixed before self-assembly at the surface, identical stacks were observed. The total inertness toward the addition of axial ligands indicates an extremely high stability of these stacks. Moreover, a remarkable feature is displayed in Figure 2a where many domains of self-assembled stacks of **1** are accompanied by relatively stable patches of nonordered surface areas. This observation indicates the presence of many nucleation sites at the surface and suggests the absence of lower-order aggregates of **1** (such as dimers) in the solution phase.

Solution-Phase Behavior. To investigate whether the stacks of **1** also exist in the absence of a potentially stabilizing surface, DLS studies were carried out (Figure S6, Supporting Information). Particles in the range of 60–100 nm were observed in a 1.1×10^{-5} M solution of **1** in dry toluene; this is in line with the size of particles observed when a dried sample of the solution was analyzed by TEM (Figure S7, Supporting Information). The addition of a very large amount of competitively binding pyridine (5×10^5 equivalents) to the analyte solution reduced the observed size to below the DLS detection limit, indicating the complete disruption of the aggregated state. These results hence indicate that also in solution a highly stable aggregate is formed based on bis-Zn(salphen) complex **1**.

Spectroscopic Studies. The dissociation of the aggregated state induced by competitive pyridine binding was then monitored in detail by UV–vis and fluorescence spectroscopy. The addition of pyridine to a solution of bis-Zn(salphen) **1** in toluene resulted in a very large increase in intensity of the UV–vis absorption maximum around $\lambda = 502$ nm (Figure 3c) and also of the fluorescence emission at $\lambda = 560$ nm (Figure S8, Supporting Information). Similar spectroscopic behavior, although far less pronounced, has been reported for related aggregate-to-monomer transitions.[9,12] In the case of mono-Zn(salphen) **8**, 10 equivalents of titrant were sufficient to

dx.doi.org/10.1021/ja3030802 | J. Am. Chem. Soc. 2012, 134, 7186–7192

disrupt the aggregated structure (Figure S9, Supporting Information). For **1** complete deaggregation could only be realized using a huge amount of 400 000 equivalents of pyridine (Figure 3c,d), thus its self-assembled state is significantly more stable compared to that of **8**. In order to estimate the stability of these stacked species in solution, the titration data were analyzed by fitting to a binding model using Specfit/32[13] as reported below.

A representative stability constant between a bis-Zn(salphen) complex and pyridine having a a 1:2 stoichiometry was derived from a titration of pyridine to tetra-*tert*-butyl bis-Zn(salphen) complex **7** (Scheme 2). For this complex, aggregation via Zn−O coordination is minimized due to the steric bulk in the 3 and 3′-positions of the salphen ligand scaffold, and hence, the Zn centers are fully accessible for pyridine coordination.[8a,14] Upon addition of pyridine, the absorption maximum at λ = 520 nm decreased, and a new maximum appeared at λ = 498 nm (Figures 3a and S10, Supporting Information). These spectral changes are completely different than those observed for complexes **1** and **3**−**6** without bulky *tert*-butyl groups in the ortho positions, and this is attributed to the absence of oligomeric species. Furthermore, clear inflection points are observed after the addition of one and two equivalents of the ligand corresponding to formation of both the 1:1 and 1:2 complexes. The data were analyzed considering three independent colored species (i.e., the "free" bis-Zn(salphen) and the 1:1 and 1:2 adducts; see Scheme 2), and this rendered an overall stability constant for the **7**·$(Py)_2$ (K_{21}) complex of 5.81×10^{11} M^{-2} (see Table 1 for K_{11} and $K_{11\rightarrow21}$ and the corrected microscopic constants and Figure S10, Supporting Information for simulated concentration profiles).

Scheme 2. Schematic Representation of the Species Involved in the Equilibria of Binding Pyridine to bis-Zn(salphen) 7[a]

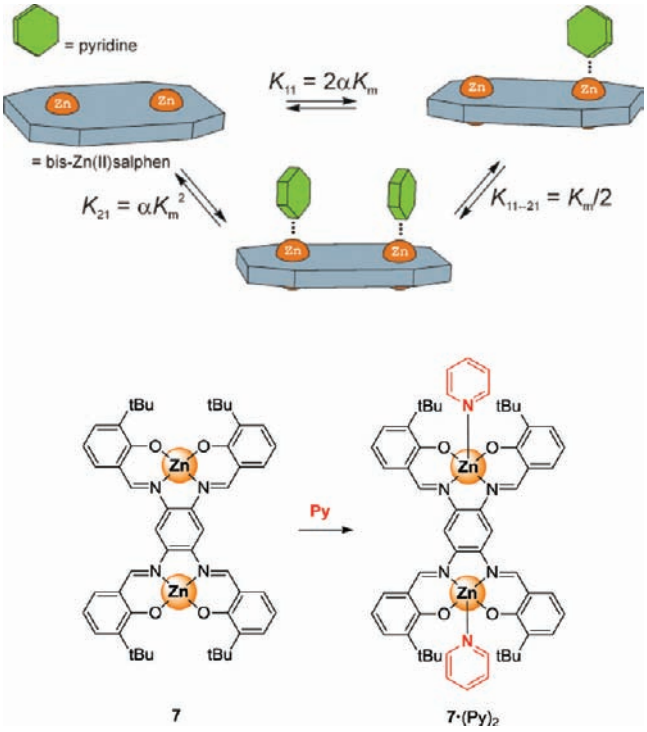

[a]The overall binding constants K_{11} and K_{21} and stepwise constant $K_{11\rightarrow21}$ are shown and related to K_m (microscopic binding constant), α (cooperativity factor), and statistical correction factors.

The pyridine titration data for C_{12}-derived bis-Zn(salphen) complex **1** were analyzed considering the binding model shown in Scheme 3, which includes three colored species (the "free" monomeric bis-Zn(salphen), the 1:2 adduct, and the oligomer designated *n*-mer). To further reduce the amount of variables, the value of K_{21} (5.81×10^{11} M^{-2}; see above) was fixed, and the absorption spectra of all species were introduced as known spectra.[15] The titration data were fitted separately for n = 2−6 (Figure 3c,d and Table 2, see also Figure S11, Supporting Information).[16] The presence of a complex with a 1:1 stoichiometry [i.e., a **1**·(Py) complex] is not likely since the binding of the second pyridine ligand is facilitated by binding of the first ligand, which decreases the intermolecular interaction between the bis-Zn(salphen) complexes.

From Figure S11, Supporting Information, one can clearly see that fitting of the data to a model for dimer formation (n = 2, Figure S11, Supporting Information) does not give a good fit. Much better fits are obtained when higher order assemblies are taken into account with an optimum around the tetramer/pentamer species (n = 4, 5; Figure 3d). At higher n-values, the quality of the binding model is reduced, because more intermediate species are excluded (for the hexamer, for example, all intermediates with $n < 6$, $n \neq 1$ are excluded in the data fit).[16] This may cause the poorer data fit for the hexameric assembly. When isodesmic behavior is assumed, the following equations can be considered:

$$M_n + M = M_{n+1}$$

$$K_{n\leftrightarrow n+1} = [M_{n+1}]/[M_n][M] = (K_n)^{1/n-1}$$

From these data we can extrapolate that every addition of monomer to a previously formed oligomer has a remarkably high association constant in the order of about 10^{20} M^{-1}. These oligomers most likely cluster in solution to give the larger particles observed by DLS and TEM.

To exclude that the long alkyl chains in the 5- and 5′-positions of the salphen scaffold are the primary cause of aggregation, we carried out the same titrations for related mono-Zn(salphen) **10** and bis-Zn(salphen) complexes **3**−**6** (Scheme 1). Interestingly, the comparison between **1** and **3**−**6** gave fairly similar results (Figure S12, Supporting Information). In the case of complexes **3**−**6**, between 75 000−400 000 equivalents of pyridine were needed to induce full deaggregation. The size of the substituents in the 3- and 3′-positions of the salphen ligand, on the other hand, proved to be more

Table 1. Macroscopic and Microscopic Binding Constants for the Binding of Pyridine to 7

K_{11} (M^{-1})	$K_{11\leftrightarrow21}$ (M^{-1})	K_{21} (M^{-2})	K_1 (M^{-1})[a]	K_2 (M^{-1})[b]	α[c]
8.79×10^5	6.61×10^5	5.81×10^{11}	4.40×10^5	1.32×10^6	3.0

[a]$K_1 = K_{11}/2$. [b]$K_2 = 2K_{11\leftrightarrow21} = 2K_{21}/K_{11}$, [c]$\alpha = K_2/K_1$; this observation of cooperativity suggests that, although bulky groups are present in the 3- and 3′-position of the ligand scaffold, a weak intermolecular interaction is present between the bis-Zn(salphen) complexes, which is broken up after binding of the first pyridine ligand.

dx.doi.org/10.1021/ja3030802 | J. Am. Chem. Soc. 2012, 134, 7186−7192

Scheme 3. Involved Species in the Titration of Pyridine to bis-Zn(salphen) Complex 1[a]

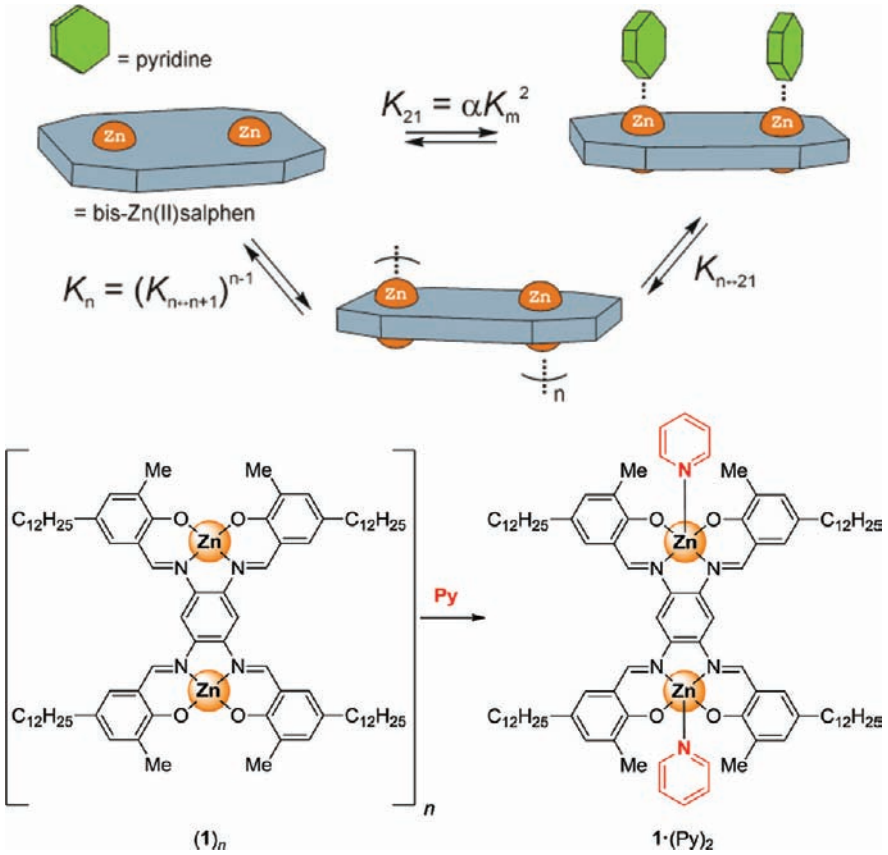

[a] K_n is the stability constant of the oligomer or n-mer, K_{21} that of the 2:1 complex and $K_{n\leftrightarrow 21}$ is the stepwise constant.

Table 2. Stability Constants for the *n*-mers Based on the Competitive Pyridine Titration of 1

n	2	3	4	5	6
K_n ($M^{-(n-1)}$)	2.23×10^{29}	5.98×10^{46}	1.85×10^{64}	6.11×10^{81}	2.11×10^{99}
error (%)	±0.087	±0.044	±0.034	±0.034	±0.037

influential. When bulky *tert*-butyl groups are introduced, no observable aggregation is noted (see compound **7**, Figure 3a,b and Figure S10, Supporting Information). This, together with the fact that no stacks are observed with STM for the bis-Ni(salphen) complex **2**,[17] clearly points to the conclusion that Zn−O interactions are the primary cause of this extremely strong aggregation.

Modeling and DFT Studies. It has been well established that mono-Zn(salphen) complexes dimerize via two μ_2-phenoxy interactions leading to the formation of a stable dimeric Zn_2O_2 core unit (Figure 4).[7,8] In order to elucidate the nature of the most likely involved coordination motifs in the self-assembled state of $(\mathbf{1})_n$, DFT minimization of a trimer (n = 3), tetramer (n = 4), and pentamer (n = 5) of **1** was performed at the level of B3LYP/6-31G* using Gaussian 09 (G09) program package[18] (Figure 5 and Figures S14−15, Supporting Information). In the case of the bis-Zn(salphen) complexes (cf., **1** and **3**−**6**), the same coordination mode (i.e., formation of dimeric Zn_2O_2 units) as observed for mono-Zn(salphen) complexes is clearly not feasible as it leads to a heavily distorted Zn_2O_2 unit and an unfavorable geometry around the Zn centers. The most efficient coordination mode involves axial coordination by a phenolate O atom of an adjacent bis-salphen molecule, forming a ladder-type structure (Figure 5c, see also

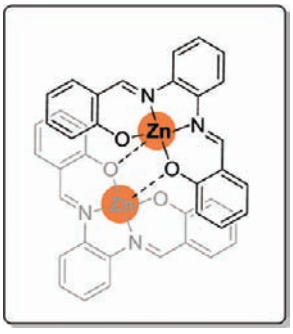

Figure 4. Dimerization of a mono-Zn(salphen) showing the typical Zn_2O_2 unit.

the STM analysis of **1**; Figure 2b). As single Zn−O interactions are prevailing, the formation of larger stacks of molecules leads to electronically more stabilized Zn centers and presumably highly stable $(Zn{-}O)_n$ oligomeric/polymeric chains. In this arrangement the length of the calculated Zn−O intermolecular coordinative bonds of 2.12−2.15 Å supports the possibility of having strong coordinative interactions between the individual bis-salphen scaffolds. This preferred coordination motif in assembled $(\mathbf{1})_n$ has been rarely observed.[19]

dx.doi.org/10.1021/ja3030802 | J. Am. Chem. Soc. 2012, 134, 7186−7192

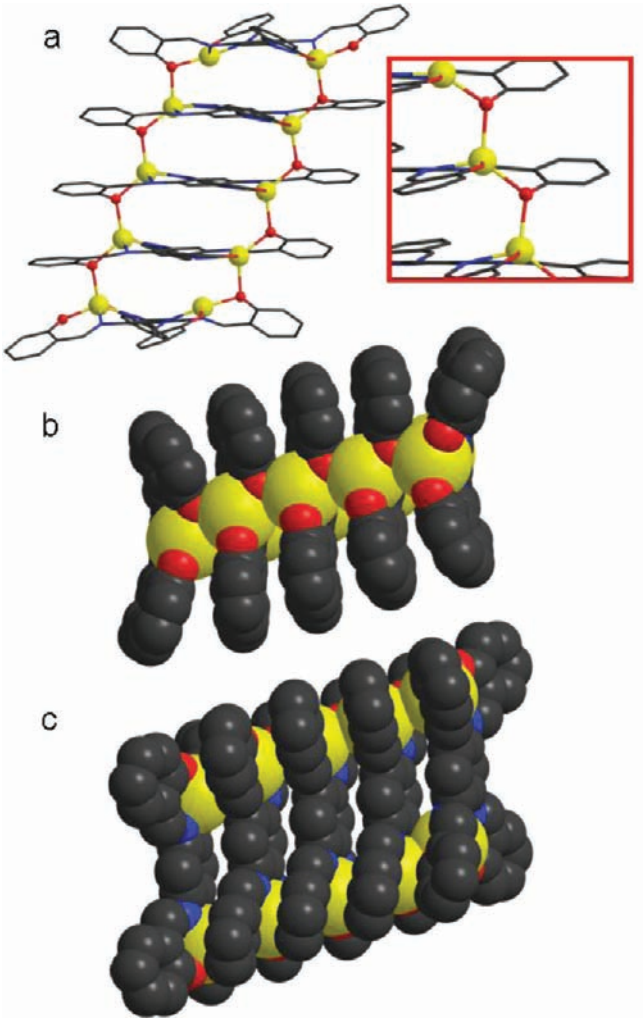

Figure 5. DFT-minimized structure for the pentameric assembly based on **1** (long tails not included). (a) Ball and stick representation of pentameric **1**, in the red inset an enlargement of the $(Zn-O)_n$ oligomeric/polymeric chains; and (b) and (c) represent space filling models from different angles.

CONCLUSIONS

In summary, the reported series of bis-Zn(salphen) complexes (**1** and **3**–**6**) show unusually strong self-assembly behavior through connecting coordination motifs that are fundamentally different from those found for self-assembled mononuclear Zn(salphen)s. All the analytical data support a highly strong and rare self-assembly behavior, and the STM imaging represents the first example of visualizing such behavior at the single-molecule level. Since Zn(salphen)s are readily available and easy to modulate synthons, their utilization gives new opportunities for the controlled fabrication of nanostructured materials driven by a tunable self-assembly process. These versatile structures are potentially useful in the creation of novel electronic and advanced opto-electronic materials.

ASSOCIATED CONTENT

Supporting Information

Detailed experimental, spectroscopic, computational, and further analytical details for the compounds described herein. This material is available free of charge via the Internet at http://pubs.acs.org.

AUTHOR INFORMATION

Corresponding Author

akleij@iciq.es; J.Elemans@science.ru.nl

Present Address

[⊥]ETH Zurich, Laboratory of Organic Chemistry, Department of Chemistry and Applied Biosciences, HCI G320 Wolfgang-Pauli-Strasse 10, CH-8093 Zurich, Switzerland.

Notes

The authors declare no competing financial interest.

ACKNOWLEDGMENTS

This work was supported by ICIQ, ICREA, and the Spanish Ministerio de Economía y Competitividad (MINECO) through project CTQ2011-27385 and an FPU fellowship to G.S.. Further support was supplied by NanoNed, the Dutch nanotechnology initiative by the Ministry of Economic Affairs, the Council for the Chemical Sciences of the Netherlands Organization through Scientific Research for a Vidi grant (700.58.423) and the European Research Council through an ERC Starting grant (NANOCAT, 259064). We also thank Prof. Pau Ballester for helpful discussions.

REFERENCES

(1) For an essay: de Greef, T. F. A.; Meijer, E. W. *Nature* **2008**, *453*, 171.

(2) (a) van Hameren, R.; van Buul, A. M.; Castriciano, M. A.; Villari, V.; Micali, N.; Schön, P.; Speller, S.; Monsù Scolaro, L.; Rowan, A. E.; Elemans, J. A. A. W.; Nolte, R. J. M. *Nano Lett.* **2008**, *8*, 253. (b) Love, J. C.; Estroff, L. A.; Kriebel, J. K.; Nuzzo, R. G.; Whitesides, G. M. *Chem. Rev.* **2005**, *105*, 1103.

(3) For some recent examples: (a) Burnworth, M.; Tang, L.; Kumpfer, J. R.; Duncan, A. J.; Beyer, F. L.; Fiore, G. L.; Rowan, S. J.; Weder, C. *Nature* **2011**, *472*, 334. (b) Cordier, P.; Tournilhac, F.; Soulié-Ziakovic, C.; Leibler, L. *Nature* **2008**, *451*, 977.

(4) (a) Screen, T. E. O.; Thorne, J. R. G.; Denning, R. G.; Bucknall, D. G.; Anderson, H. L. *J. Am. Chem. Soc.* **2002**, *124*, 9712. (b) Drobizhev, M.; Stepanenko, Y.; Rebane, A.; Wilson, C. J.; Screen, T. E. O.; Anderson, H. L. *J. Am. Chem. Soc.* **2006**, *128*, 12432.

(5) (a) Brunsveld, L.; Vekemans, J. A. J. M.; Hirschberg, J. H. K. K.; Sijbesma, R. P.; Meijer, E. W. *Proc. Natl. Acad. Sci. U.S.A.* **2002**, *99*, 4977. (b) Sijbesma, R. P.; Beijer, F. H.; Brunsveld, L.; Folmer, B. J. B.; Hirschberg, J.; Lange, R. F. M.; Lowe, J. K. L.; Meijer, E. W. *Science* **1997**, *278*, 1601. (c) *Advances in Polymer Science – Hydrogen Bonded Polymers*; Binder, W., Ed.; Springer: Berlin, Germany, 2007; Vol. *207*.

(6) (a) Sprafke, J. K.; Odell, B.; Claridge, T. D. W.; Anderson, H. L. *Angew. Chem., Int. Ed.* **2011**, *50*, 5572. (b) Helmich, F.; Lee, C. C.; Nieuwenhuizen, M. M. L.; Gielen, J. C.; Christianen, P. C. M.; Larsen, A.; Fytas, G.; Leclère, P. E. L. G.; Schenning, A. P. H. J.; Meijer, E. W. *Angew. Chem., Int. Ed.* **2010**, *49*, 3939. (c) Michelsen, U.; Hunter, C. A. *Angew. Chem., Int. Ed.* **2000**, *39*, 764. (d) O'Sullivan, M. C.; Sprafke, J. K.; Kondratuk, D. V.; Rinfray, C.; Claridge, T. D. W.; Saywell, A.; Blunt, M. O.; O'Shea, J. N.; Beton, P. H.; Malfois, M.; Anderson, H. L. *Nature* **2011**, *469*, 72. (e) Suijkerbuijk, B. M. J. M.; Tooke, D. M.; Spek, A. L.; van Koten, G.; Klein Gebbink, R. J. M. *Chem. Asian J.* **2007**, *2*, 889. (f) Merlau, M. L.; del Pilar Mejia, M.; Nguyen, S. T.; Hupp, J. T. *Angew. Chem., Int. Ed.* **2001**, *40*, 4239.

(7) Elemans, J. A. A. W.; Wezenberg, S. J.; Escudero-Adán, E. C.; Benet-Buchholz, J.; den Boer, D.; Coenen, M. J. J.; Speller, S.; Kleij, A. W.; de Feyter, S. *Chem. Commun.* **2010**, *46*, 2548.

(8) (a) Martínez Belmonte, M.; Wezenberg, S. J.; Haak, R. M.; Anselmo, D.; Escudero-Adán, E. C.; Benet-Buchholz, J.; Kleij, A. W. *Dalton Trans.* **2010**, *39*, 4541. (b) Kleij, A. W. *Dalton Trans.* **2009**, 4635.

(9) Salassa, G.; Castilla, A. M.; Kleij, A. W. *Dalton Trans.* **2011**, *40*, 5236.
(10) (a) Escudero-Adán, E. C.; Martínez Belmonte, M.; Martin, E.; Salassa, G.; Benet-Buchholz, J.; Kleij, A. W. *J. Org. Chem.* **2011**, *76*, 5404. (b) Escudero-Adán, E. C.; Benet-Buchholz, J.; Kleij, A. W. *Inorg. Chem.* **2008**, *47*, 4256.
(11) (a) Elemans, J. A. A. W.; Lensen, M. C.; Gerritsen, J. W.; van Kempen, H.; Speller, S.; Nolte, R. J. M.; Rowan, A. E. *Adv. Mater.* **2003**, *15*, 2070. (b) Lensen, M. C.; Elemans, J. A. A. W.; van Dingenen, S. J. T.; Gerritsen, J. W.; Speller, S.; Rowan, A. E.; Nolte, R. J. M. *Chem.– Eur. J.* **2007**, *13*, 7948.
(12) (a) Ma, C. T. L.; MacLachlan, M. J. *Angew. Chem., Int. Ed.* **2005**, *44*, 4178. (b) Consiglio, G.; Failla, S.; Finocchiaro, P.; Oliveri, I. P.; Purello, R.; Di Bella, S. *Inorg. Chem.* **2010**, *49*, 5134. (c) Leung, A. C. W.; MacLachlan, M. J. *J. Mater. Chem.* **2007**, *17*, 1923. (d) Consiglio, G.; Failla, S.; Finocchiaro, P.; Oliveri, I. P.; Di Bella, S. *Dalton Trans.* **2012**, *41*, 387.
(13) (a) *Specfit/32*, version 3.0; Spectra Software Associates: Bradford-on-Avon, U.K., 2005. Specfit/32 is a multivariate data analysis program for modeling and fitting multiwavelength titration data sets giving more reliable parameters than single-wavelength fits. For software details and the related nonlinear algorithms see: (b) Gampp, H.; Maeder, M.; Meyer, C. J.; Zuberbühler, D. A. *Talanta* **1985**, *32*, 95. (c) Gampp, H.; Maeder, M.; Meyer, C. J.; Zuberbühler, D. A. *Talanta* **1986**, *33*, 943.
(14) Kleij, A. W.; Kuil, M.; Lutz, M.; Tooke, D. M.; Spek, A. L.; Kamer, P. J. C.; van Leeuwen, P. W. N. M.; Reek, J. N. H. *Inorg. Chim. Acta* **2006**, *359*, 1807.
(15) *n*-mer: initial UV–vis spectrum, 1:2 and free complex: final UV–vis spectrum of the titration data. Note that the free complex will be virtually absent throughout the titration and that its spectrum is thus arbitrary for the data fit. Nevertheless, as can be deduced from titration with *tetra*-tert-butyl complex **7**, it will reasonably equal the absorption spectrum of the 2:1 complex in comparison to the spectrum of the *n*-mer.
(16) Introduction of multiple *n*-values in the same data fit led to too many free parameters in Specfit/32 and therefore only a single *n*-value could be chosen in each fitting procedure.
(17) It is important to note here that mono-Ni complex **9** showed virtually no change in absorption behavior upon titration with pyridine (Figure S13), suggesting that this complex is unable to have intermolecular Ni–O interactions.
(18) Frisch, M. J.; Trucks, G. W.; Schlegel, H. B.; Scuseria, G. E.; Robb, M. A.; Cheeseman, J. R.; Scalmani, G.; Barone, V.; Mennucci, B.; Petersson, G. A.; Nakatsuji, H.; Caricato, M.; Li, X.; Hratchian, H. P.; Izmaylov, A. F.; Bloino, J.; Zheng, G.; Sonnenberg, J. L.; Hada, M.; Ehara, M.; Toyota, K.; Fukuda, R.; Hasegawa, J.; Ishida, M.; Nakajima, T.; Honda, Y.; Kitao, O.; Nakai, H.; Vreven, T.; Montgomery, J. A., Jr.; Peralta, J. E.; Ogliaro, F.; Bearpark, M.; Heyd, J. J.; Brothers, E.; Kudin, K. N.; Staroverov, V. N.; Kobayashi, R.; Normand, J.; Raghavachari, K.; Rendell, A.; Burant, J. C.; Iyengar, S. S.; Tomasi, J.; Cossi, M.; Rega, N.; Millam, J. M.; Klene, M.; Knox, J. E.; Cross, J. B.; Bakken, V.; Adamo, C.; Jaramillo, J.; Gomperts, R.; Stratmann, R. E.; Yazyev, O.; Austin, A. J.; Cammi, R.; Pomelli, C.; Ochterski, J. W.; Martin, R. L.; Morokuma, K.; Zakrzewski, V. G.; Voth, G. A.; Salvador, P.; Dannenberg, J. J.; Dapprich, S.; Daniels, A. D.; Farkas, Ö. ; Foresman, J. B.; Ortiz, J. V.; Cioslowski, J.; Fox, D. J. *Gaussian 09* , revision 7.0; Gaussian, Inc.: Wallingford, CT, 2009.
(19) MacLachlan reported on a mono-nuclear Zn(salphen) system able to self-assemble up to a nonamer displaying a coordinative $[Zn–O]_n$ chain. Hui, J. K.-H.; Yu, Z.; MacLachlan, M. J. *Angew. Chem., Int. Ed.* **2007**, *46*, 7980.